Vevek, U.S., Zang, B. & New, T.H. J Sci Comput (2018). https://doi.org/10.1007/s10915-018-0803-x

On alternative setups of the double Mach reflection problem

U S Vevek, Zang B. and New T. H.*

School of Mechanical and Aerospace Engineering, Nanyang Technological University
50 Nanyang Avenue, Singapore 639798

Abstract

The double Mach reflection (DMR) problem is an important test case for the assessment of the resolution of Euler codes. The initial and boundary conditions specified in the conventional setup of the problem result in formation of undesirable numerical artefacts which interfere with the solution. In this study, two alternative setups are proposed to prevent the manifestations of such artefacts. The first setup involves modifying the computational domain to simplify the boundary conditions while the second setup involves modifying the initial conditions to make the problem more conducive to run on uniform Cartesian grids and foregoing the problematic boundary conditions altogether. Both setups employ a modified two-step initialization procedure to obtain clean, artefact-free results. These methods are robust and easy to implement. The DMR problem was simulated using a 7^{th} order finite-volume WENO-based solver developed using OpenFOAM to demonstrate that the proposed methods can be used for the assessment of higher order methods. The proposed methods have yielded good results and complete removal of the artefacts is observed in some cases. The simulations were performed with two different numerical flux schemes to determine the dependency of the flux schemes on the performance of the setups. Lastly, the second setup was found to be superior than the first one in terms of effectively removing the numerical artefacts.

Keywords: double Mach reflection, numerical test, boundary conditions, high resolution schemes

*Corresponding author: dthnew@ntu.edu.sg

Vevek, U.S., Zang, B. & New, T.H. J Sci Comput (2018). https://doi.org/10.1007/s10915-018-0803-x

1 Introduction

1.1 Motivation

The double Mach reflection (DMR) problem was originally proposed by Woodward and Colella [1] as a numerical test to assess the fidelity of Euler codes. It involves a Mach 10 shock colliding with a ramp inclined 30° counter-clockwise to the shock propagation direction. Upon impact, a self-similar structure (see Figure 1) forms over the ramp and grows in size as the shock propagates to the right. The flow structure consists of two triple points T and T′, each of which is a confluence of three shocks and a slip line (for further details on the analytical solution, refer to [2]). In addition to the complicated shock reflection pattern, the DMR problem has several notable features such as the barely noticeable weak secondary slip line s', the wall-adjacent jet and the unstable rollups of the primary slip line s, which provide a true test of several aspects of the numerical scheme. In particular, the extent of detail captured in the rollups of s is often viewed as a measure of the extent of numerical viscosity of a given scheme [3-7]. Overall, the DMR problem serves as an excellent two-dimensional test case to benchmark Euler codes.

The current study is motivated by the work of Kemm [8] who provided a lucid account of the numerical artefacts produced when simulating the DMR problem and their causes. Upon investigating the hypotheses of Woodward and Colella [1] and Rider, et al. [9], Kemm concluded that while the artefact arising due to top boundary condition could be shifted away from the region of interest by enlarging the computational domain in the direction normal to the ramp, the artefact arising due to the sharp initialization of the incident shock could not be eliminated at all. The presence of such numerical artefacts may produce undesirable results when one attempts to validate newly developed Euler codes using DMR as a test case. In particular, resolution of the secondary slip line s' is considered to be a main challenge for

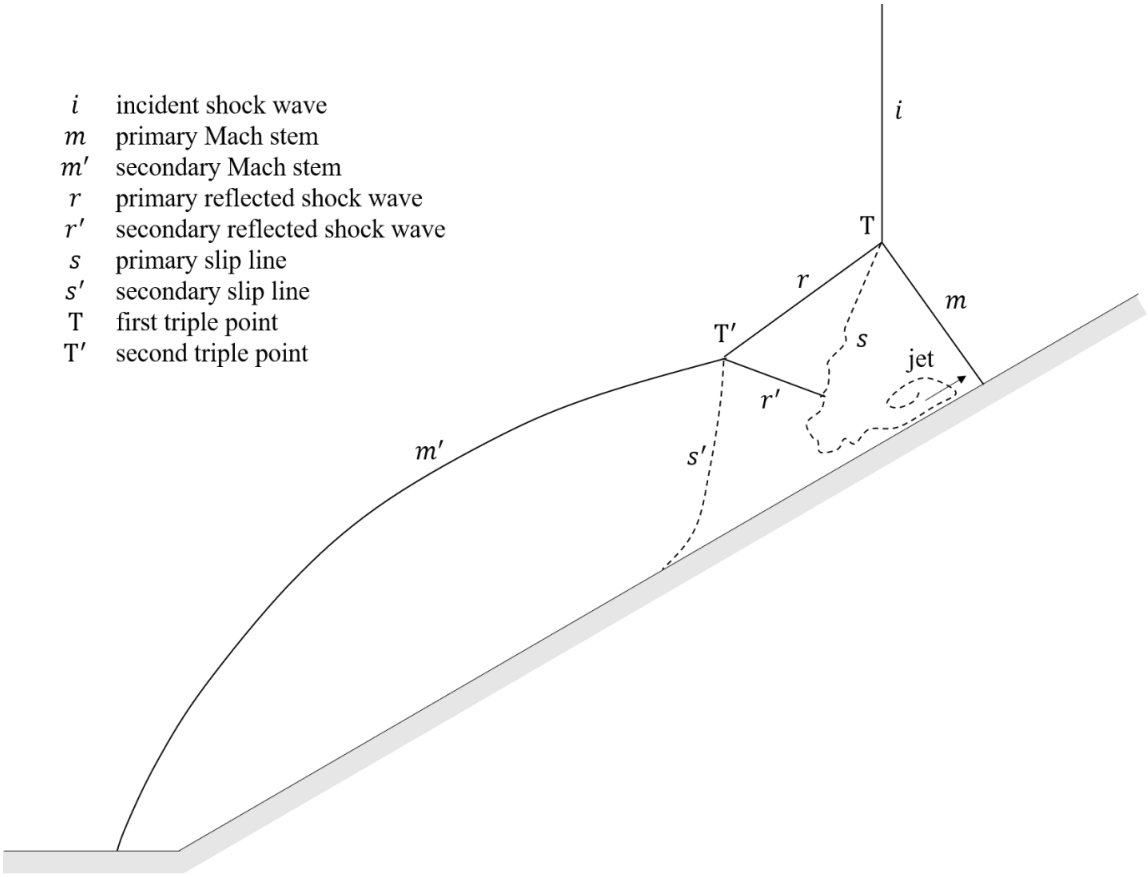

Figure 1: Schematic of the self-similar structure of the DMR problem.

numerical schemes. However, the numerical artefacts tend to distort the solution in the vicinity of s'. Therefore, the main motivation of the present study is to propose alternative setups of the DMR problem to remove the numerical artefacts so that it serves as a good test of the accuracy of the numerical schemes in capturing the slip lines. A secondary motivation is that, being quite general, the proposed strategies may be applied to other cases facing similar problems which involve sharp initialization and/or tracking an oblique discontinuity along a boundary.

1.2 Problems with the conventional setup

In the conventional setup of the DMR problem (Figure 4), the computational domain is a $[0,4]\times[0,1]$ rectangle discretized into a uniform Cartesian grid. The orthogonal grid provides the perfect and most fundamental test environment for the assessment of numerical schemes.

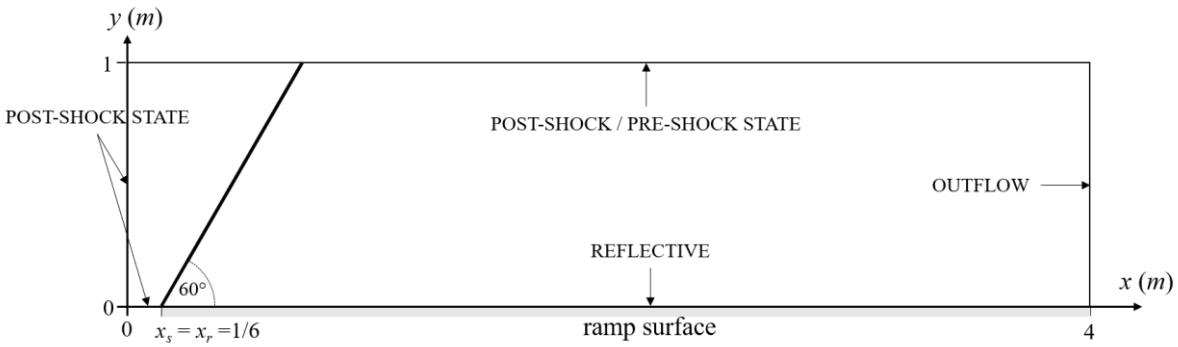

Figure 2: Schematic of the computational domain conventional setup with boundary conditions. Initial location of shock marked by thick line.

The ramp surface lies along the bottom boundary and extends to the right boundary starting from $x = x_r$. The test case is initialized with the shock inclined 60° to the horizontal, intersecting the bottom boundary at $x = x_s$. In the conventional setup, the initial shock is positioned at the foot of the ramp, i.e. $x_s = x_r$, and x_r is chosen to be 1/6. The pre- and post-shock conditions are $(\rho, p, u, v)_0 = (1.4, 1, 0, 0)$ and $(\rho, p, u, v)_1 = \left(8, 116.5, 4.125\sqrt{3}, -4.125\right)$, respectively. Here, the variables carry their usual units. At the bottom boundary, a reflecting boundary condition is specified along the ramp surface $x \in [x_r, 4]$ while the post-shock state is specified along $x \in [0, x_r]$. The post-shock state is also specified along the left boundary while an outflow/Neumann boundary is specified along the right. At the top boundary, the respective state values are prescribed in a time dependent manner by tracking the shock exactly [1, 4]. The simulation is run until $t = 0.2s$.

The DMR problem was simulated using the above setup at two grid resolutions, $\Delta = 1/120$ and $\Delta = 1/240$, with 7th order WENO scheme (refer to Section 2.4 for solver description). These grid resolutions are similar to those employed by Kemm [8] and Shi, et al. [6]. The results are shown in Figure 3 using contours of the vertical momentum ρv. Notice that the numerical artefact lies very close to s', especially for $\Delta = 1/120$, and it does not vanish as the

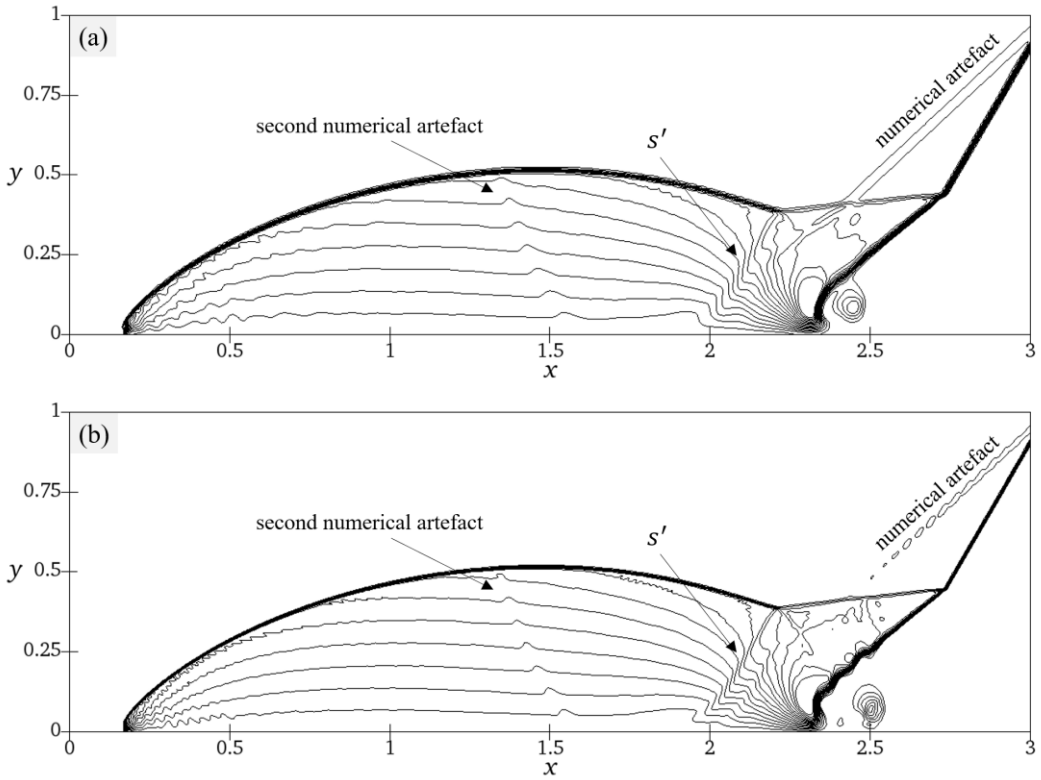

Figure 3: DMR cases were simulated using conventional setup with HLL flux for (a) Δ=1/120 and (b) Δ=1/240. 16 evenly spaced contours of ρv from -2 to -32 are used.

grid is refined. A *second* numerical artefact can also be clearly observed stemming from the bottom boundary up to secondary Mach stem in the solution.

The source of the problem lies in the sharp initial shock profile. It is well known that all shock capturing methods smear a moving shock over several cells [10]. When initialized with a sharp profile, such as in this case, spurious waves are generated as the numerical scheme attempts to smear the shock. In this case, these waves trail behind the smeared shock. Woodward and Colella [1] called this the "starting error". The situation is further exacerbated by the boundary condition at the top which attempts to specify a sharp *un-smeared* shock. This causes the first trailing wave to be anchored to the shock at the top boundary and eventually becomes the numerical artefact. Similarly, the second trailing spurious wave was found to be responsible for the second numerical artefact. Therefore, the artefacts arise due to

the interaction of two factors: the sharp shock profile used as initial condition and the sharp transition prescribed by the top boundary condition.

Kemm [8] attempted to alleviate the problem by linearly smearing the initially-sharp shock profile and applying an oblique extrapolation at the top boundary but found that both approaches made the artefact even more prominent. The set of intermediate states within the smeared shock profile is not a fixed one and the smeared profile essentially depends on the mesh and the numerical schemes used, which is possibly why rectifications using linear smearing did not perform as well as expected. Furthermore, for a given combination of mesh and numerical scheme, the intermediate states across the shock profile evolve over time. Therefore, explicit smearing of the initial shock profile will not be effective against eliminating the artefacts unless the profile happens to be consistent with the mesh and numerical scheme. Similarly, any boundary condition that is not mindful of the shock smearing will also be ineffective.

2 Numerical procedures

Based on issues identified with both the initial and boundary conditions associated with the DMR test case from the previous section, a two-step initialization procedure and two different setups of boundary treatment for the DMR problem are proposed here.

2.1 Two-step initialization

The proposed initialization procedure is slightly more elaborate than in the conventional setup but it may be unavoidable if one seeks to obtain results free of numerical artefacts. The first step of the initialization is similar to the conventional setup, whereby a sharp shock profile is initialized at $t = 0$. However, unlike in the original setup, the shock is not positioned

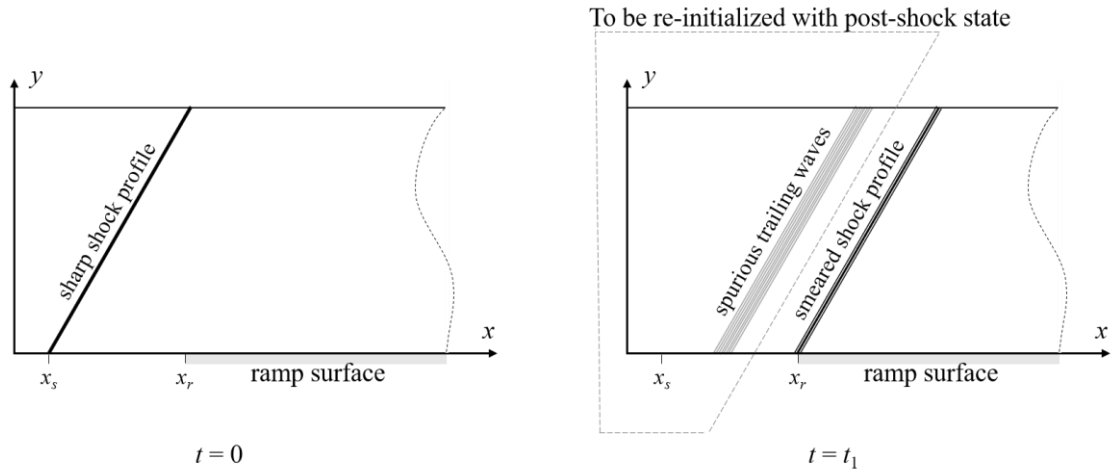

Figure 4: Diagram of two-step initialization procedure. (Left) Step 1: initialize with sharp profile, (Right) Step 2: re-initialize region to the left of smeared shock profile with post-shock state.

at the foot of the ramp but displaced a certain distance to the left, i.e. $x_s < x_r$ (see Figure 4). The simulation is then run up to $t = t_1$ to allow the shock to propagate to the right without obstruction. During this period, the shock would have been properly smeared and the trailing spurious waves would have been generated. x_s and t_1 are determined in such a way that at the end of t_1, the smeared shock just impinges (or is about to impinge) upon the ramp and the trailing spurious waves lie well-clear of the shock so that the domain can be safely re-initialized in the second step without affecting the shock.

In the second step of the initialization, the region corrupted by the numerical noise is re-initialized with the post-shock state (see Figure 4). This step should not be performed at the exact shock position to avoid any modifications to the smeared shock profile; instead, it should be applied starting from a location that is a few cells to the left of the shock location. It is emphasized that this is the only additional step required in this two-step initialization and that it adds little to the computational cost. After this step, the simulation is run as per normal until $t = t_2$ so that the solution reaches a similar end state as the conventional run. In this study, the ramp surface extends to the right from the origin, i.e. $x_r = 0m$. The initial shock is

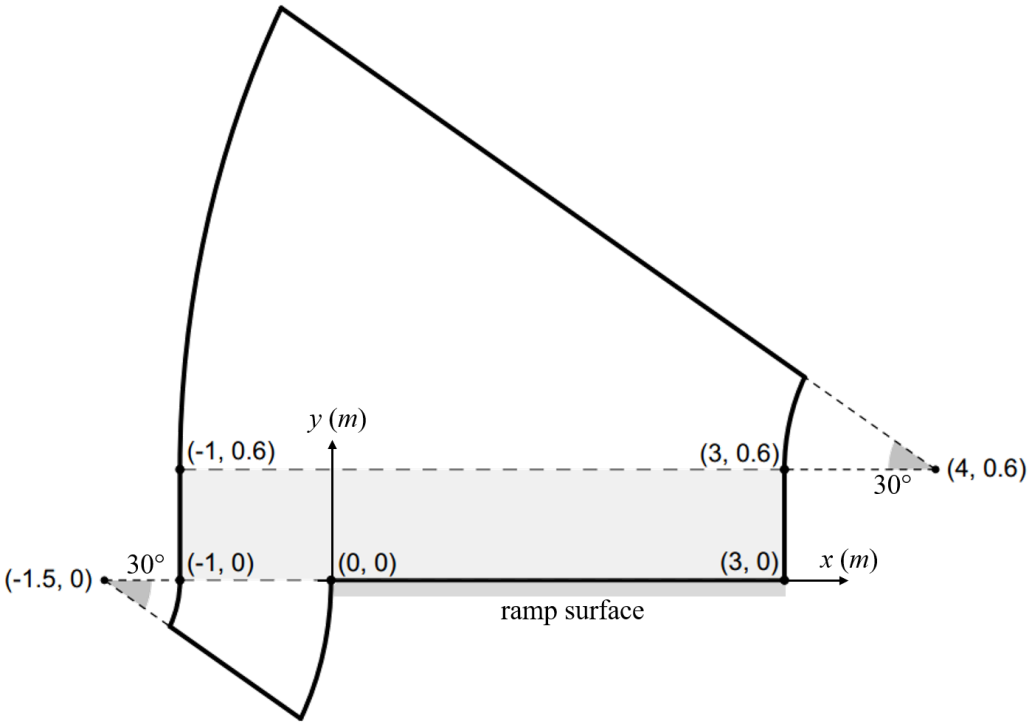

Figure 5: Schematic of the modified computational domain of first alternative setup

located at $x_s = -0.9m$ so that the shock just impinges on the ramp at a particularly convenient time of $t_1 = 0.08s$. While locating the initial shock closer to the ramp reduces t_1, it may not guarantee sufficient separation between the smeared shock and the band of trailing spurious waves for safe re-initialization. On the other hand, positioning the initial shock further to the left will not only increase t_1 but will also require the domain to be extended further to the left. Finally, upon re-initialization, the simulation is run till $t_2 = 0.27s$.

2.2 First setup: modified computational domain

The motivation behind modifying the computational domain is the observation that a simple Neumann boundary condition allows the propagation of a shock that is normal to the boundary without interfering with the numerical smearing in any way. Hence, it does not generate any numerical artefacts. Therefore, the top boundary of the modified computational domain has been designed to slope down at an angle of 30° measured clockwise from the

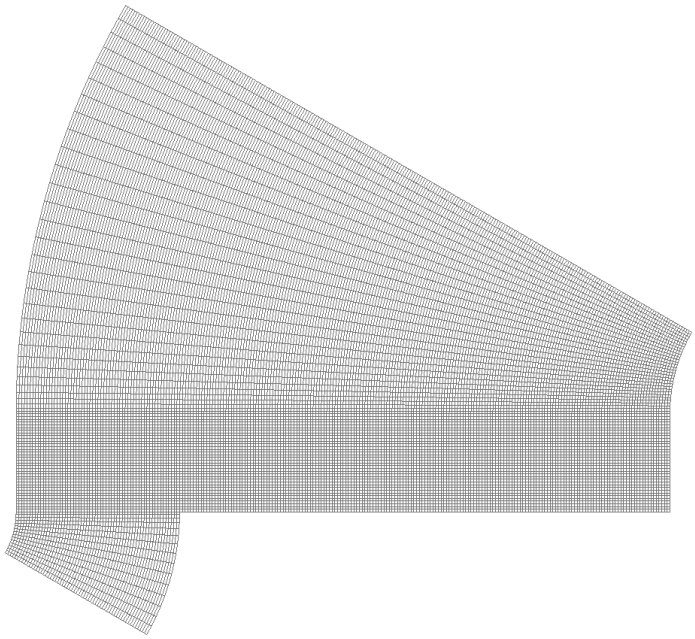

Figure 6: Coarse grid of modified computational domain of first alternative setup

horizontal as shown in Figure 5 so that it always remains normal to incident shock. Since the shock is required to travel to the right without obstruction until t_1, the left portion of the bottom boundary is also modified to slope down parallel to the top boundary.

Based on the results shown in Figure 3, it can be observed that all the prominent features of the solution, such as the shock reflections and slip lines, lie approximately between $y \in [0, 0.5]$. Thus, with a small allowance of $0.1m$ in the y direction, a $[-1, 3]\times[0, 0.6]$ rectangle was included in the computational domain (see light grey region in Figure 5). This rectangular region can be discretized using a uniform Cartesian grid as in the conventional setup to ensure that no loss of accuracy occurs. The slanted top and bottom boundaries are connected to the rectangular region of interest using circular arcs to minimize grid skewness which is essential to maintain a high degree of accuracy in those portions as well. A coarse grid using $\Delta = 1/60$ in the Cartesian grid portion is shown in Figure 6.

For $\Delta = 1/240$, the grid for this setup has nearly 272k cells which is only slightly larger than

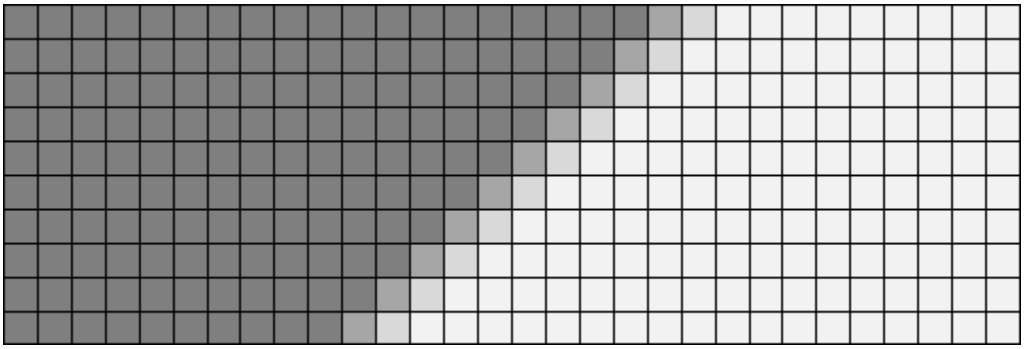

Figure 7: Periodic nature of smeared 45° oblique shock solution on a uniform grid

the conventional setup which has approximately 230k cells. Extending the computational domain in the vertical direction as suggested by Kemm [8], despite having the advantage of preserving the Cartesian grid, doubles the number of cells and does not remove the numerical artefacts. While this domain has the advantage of simplified boundary conditions, the non-Cartesian portions of the grid may not be optimal for some applications. Therefore, in the second setup, the uniform Cartesian grid is retained by modifying the initial shock orientation.

2.3 Second setup: modified initial shock orientation

To understand the reasoning behind modifying the initial shock orientation, consider the scenario of a shock inclined at 45° to the horizontal travelling to the right *without* any obstruction. When solving this problem on a uniform Cartesian grid, the smeared shock profile will be identical along each row of cells except for a shift to the left or right (see Figure 7). Using the (i, j) notation for the two-dimensional Cartesian grid, one can arrive at the following relationship

$$\phi_{i,j} = \phi_{i+k,j+k} \text{ where } k = \pm 1, \pm 2 \cdots \tag{1}$$

where ϕ may refer to any solution variable such as ρ, p, etc.

By the same reasoning, consider a shock which makes an angle of θ with the horizontal and further assume that $\tan\theta$ is a rational number, i.e. $\tan\theta = Y/X$ where X and Y are integers. In this case, Eq. (1) can be modified to become the following.

$$\phi_{i,j} = \phi_{i+kX,\, j+kY} \text{ where } k = \pm 1, \pm 2 \cdots \tag{2}$$

For the DMR problem, the solution close to the top boundary is essentially the solution for a travelling oblique shock because the influence of the ramp would not be 'felt' by the region throughout the simulation time. Therefore, the afore-mentioned periodicity of the numerical solution for a travelling oblique shock could be exploited to avoid specifying *any* boundary condition at the top boundary for the DMR problem.

Unfortunately, the original initial conditions of the DMR problem do not allow for such periodicity since $\tan 60° = \sqrt{3}$ is not a rational number. Therefore, a slight change in the initial conditions is proposed whereby the shock makes an angle $\tilde{\theta}$ such that $\tan\tilde{\theta} = 7/4 = 1.75 \approx \tan 60.25°$. Thus, in this case, the numerical solution in a few rows of cells adjacent to the top boundary can be replaced with the interior solution values as shown below.

$$\phi_{i,j}^{top} = \phi_{i-4,\, j-7} \tag{3}$$

Therefore, no boundary condition is necessary at the top. A similar treatment must be applied to a few rows of cells close to bottom boundary before the shock impinges on the ramp.

$$\phi_{i,j}^{bottom} = \phi_{i+4,\, j+7} \tag{4}$$

The number of rows to be replaced depends on the spatial reconstruction scheme. For instance, for the 7^{th} order WENO scheme that was used in this study, the spatial

reconstruction stencil extends four cells on either side of the cell interface. Therefore, the solution in four rows of cells adjacent to the top and bottom boundaries was replaced with the corresponding solution from the interior. Take note that the pre-shock density and pressure are the same as the conventional setup whereas the post-shock velocities are given by $(u, v)_1 = \left(8.25\sin\left(60.25^\circ\right), -8.25\cos\left(60.25^\circ\right)\right)$.

2.4 Solver description

An in-house finite volume code developed based on OpenFOAM was used to simulate the DMR test case. A 7th order WENO scheme was chosen to show that the setups can be used effectively with high order schemes. The WENO methodology is adapted from Jiang and Shu [11]. Similar treatments can be found in [12, 13]. Note that the WENO reconstruction is performed along local face-normal direction and, hence, does not require a fully Cartesian or uniform grid. Furthermore, WENO reconstruction in characteristic space is employed near shocks to alleviate post-shock oscillations typically associated with higher-order reconstruction on primitive variables. The solver uses a 3rd order TVD Runge-Kutta method [14] for time marching of the solution. Last but not least, at each time step, the fluxes across the faces are computed through either Rusanov-type [15] or HLL-type [16] flux.

3 Results & discussions

The results obtained using the first setup are shown in Figures 8 and 9 using contours of vertical momentum ρv. Comparing these results with those obtained using the conventional setup (Figure 3), it is clear that the use of the modified computational domain has largely removed the numerical artefacts. Some residual noise was observed in the region above the incident shock in all four cases regardless of the mesh resolutions and numerical flux. schemes. However, they were too weak to cause any observable distortions in the solution

near the secondary slip line s'. It is speculated that the non-uniform grid portions are causing the numerical smearing process to continue throughout the simulation leading to the constant generation of noise. Nonetheless, the first setup was able to remove the second numerical artefact completely in all four cases.

The results obtained using the second setup are shown in Figures 10 and 11 using contours of vertical momentum ρv. It can be observed that the second setup is able to eliminate both numerical artefacts completely in all four cases. In addition, very little residual numerical noise was found in the final solutions. This lends further credibility to the authors' earlier speculation that the non-uniform portions of the grid in the first setup might be responsible for the generation of more numerical noise and the distorted secondary slip lines. It is apparent that the secondary slip lines have been captured without any distortion.

The density contour plots are shown in Figure 12 comparing the results of the conventional and the proposed setups (results only for $\Delta = 1/240$ and HLL flux are shown). Note that the weak secondary slip line s' is not at all visible in the density contour plots. The sizes of the smallest rollup captured by the setups are about the same which indicates that the proposed setups do not sacrifice accuracy. It is worth noting that the modified shock orientation in the second setup still preserves all the essential features of the flow and, hence, can be used for the assessment of Euler codes. The two-step initialization procedure is crucial to eliminating the numerical artefacts but it must be highlighted that there are no strict rules to determine the region corrupted by the numerical noise that needs to be re-initialized with the post-shock state. Fortuitously, it was observed that the results are not too sensitive to this choice as long as the region is at least 3-4 cells to the left of the shock position.

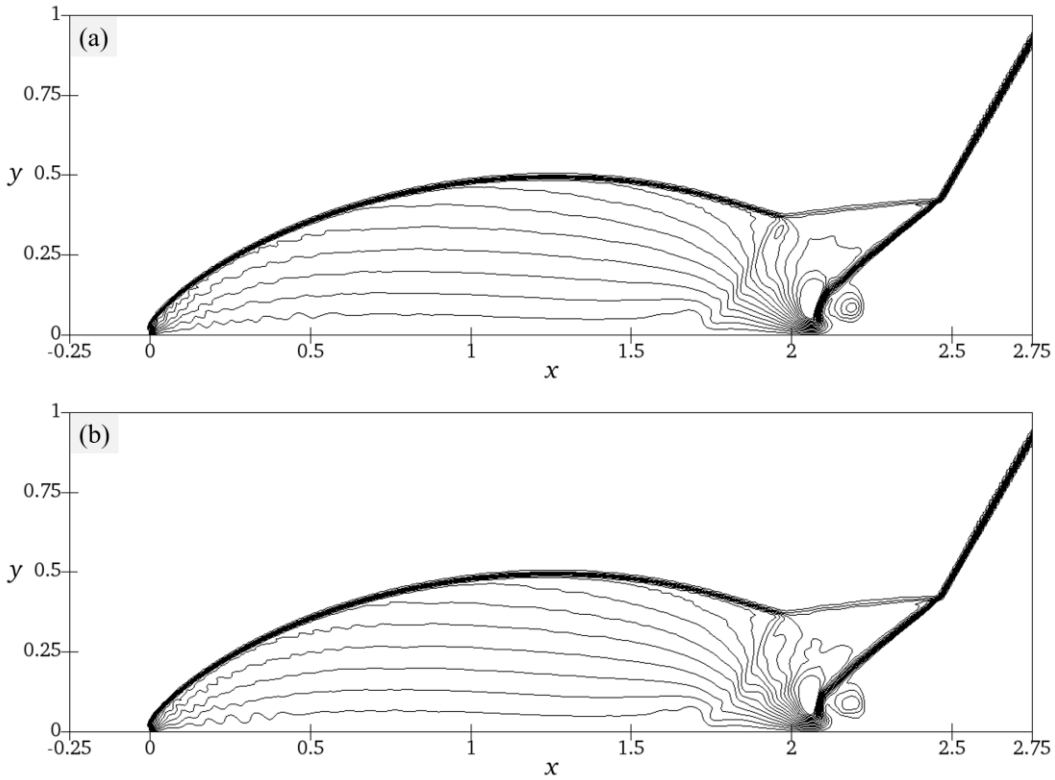

Figure 8: DMR cases were simulated using first setup with Δ=1/120 using (a) HLL flux and (b) Rusanov flux. 16 evenly spaced contours of vertical momentum ρv from -2 to -32 are used.

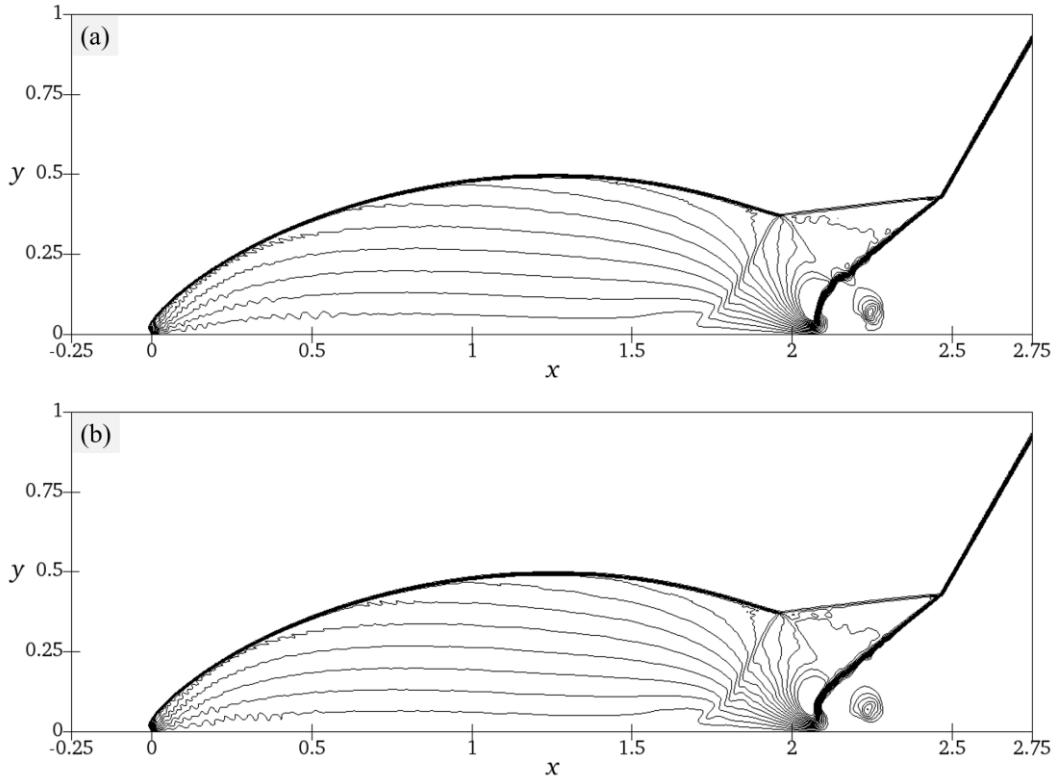

Figure 9: DMR cases were simulated using first setup with Δ=1/240 using (a) HLL flux and (b) Rusanov flux. 16 evenly spaced contours of vertical momentum ρv from -2 to -32 are used.

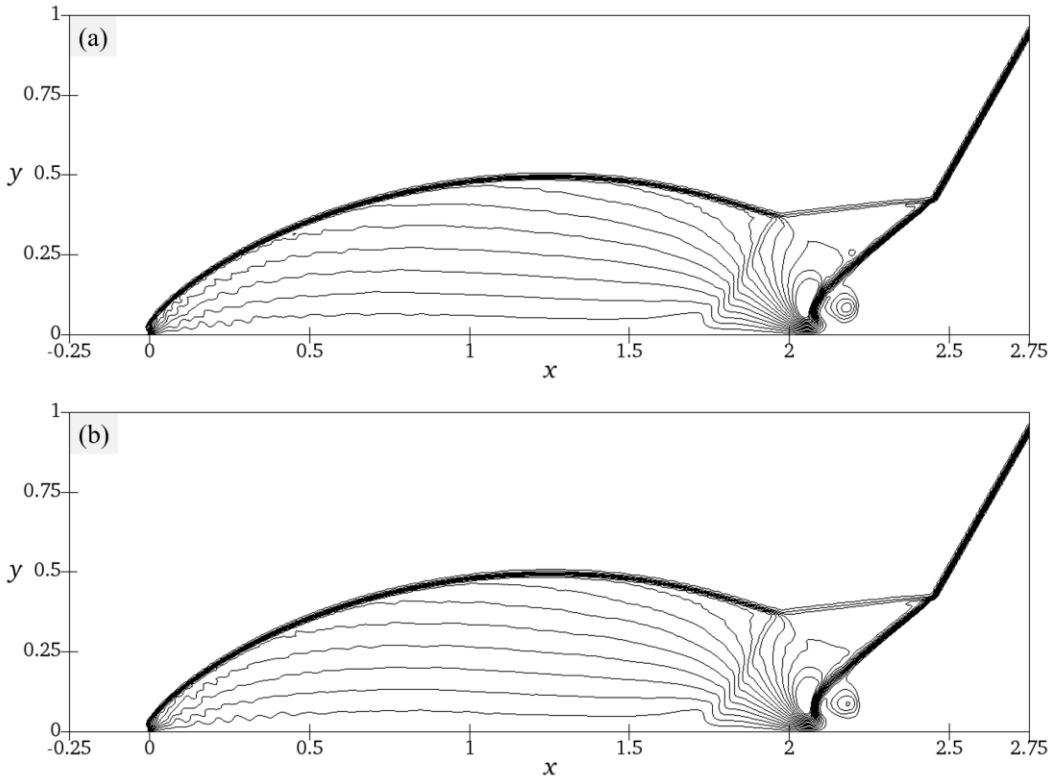

Figure 10: DMR cases were simulated using first setup with Δ=1/120 using (a) HLL flux and (b) Rusanov flux. 16 evenly spaced contours of vertical momentum ρv from -2 to -32 are used.

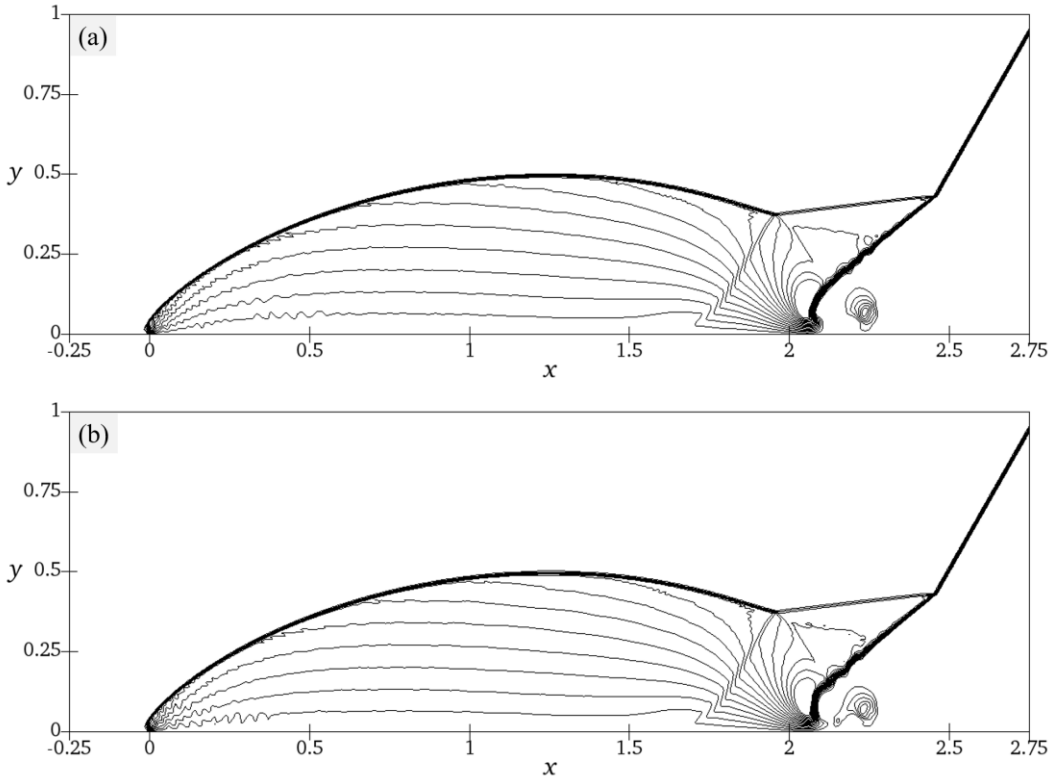

Figure 11: DMR cases were simulated using first setup with Δ=1/240 using (a) HLL flux and (b) Rusanov flux. 16 evenly spaced contours of vertical momentum ρv from -2 to -32 are used.

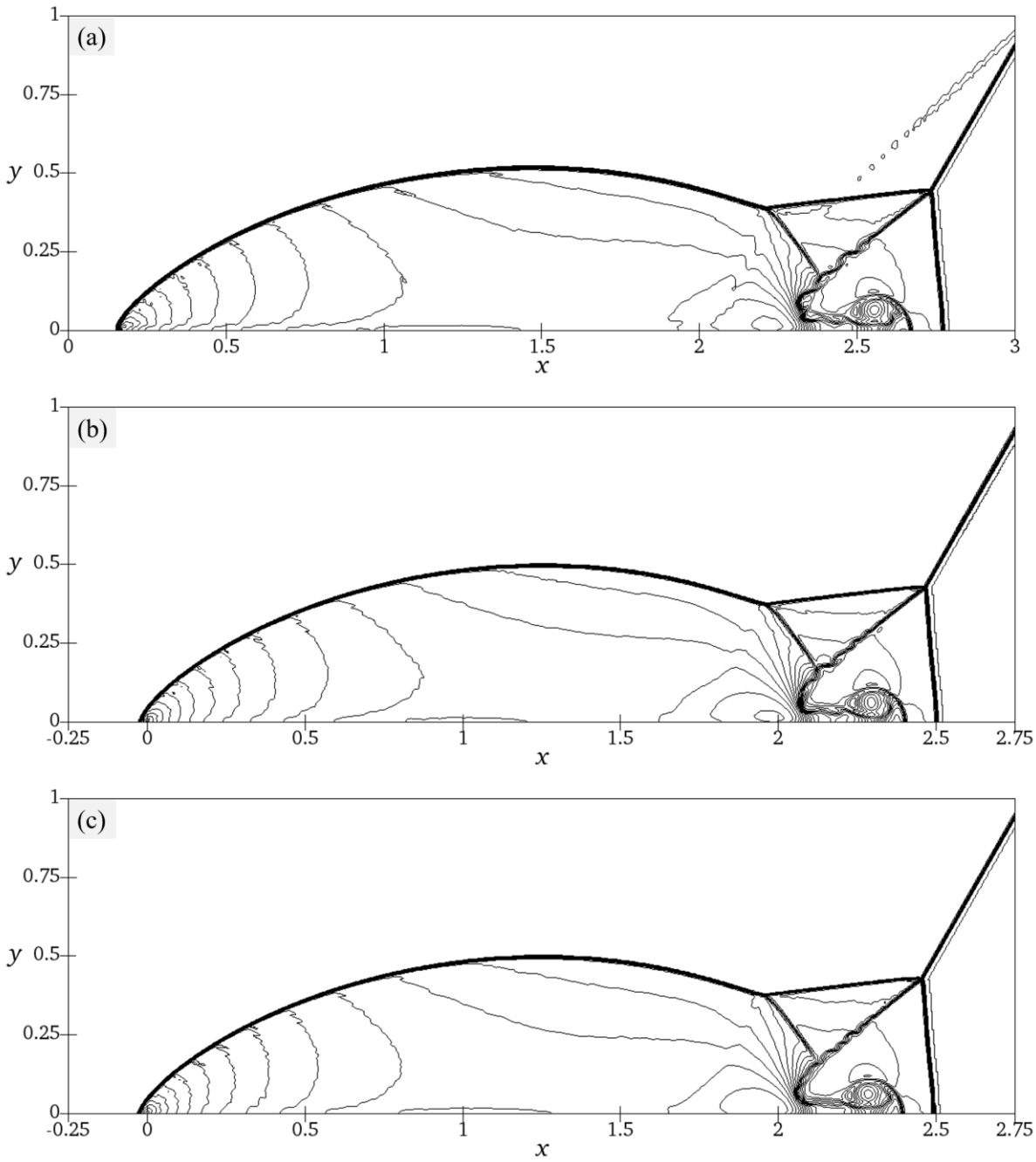

Figure 12: DMR cases were simulated using HLL flux with Δ=1/240. (a) Conventional setup, (b) first setup, (c) second setup. 41 evenly spaced contours of ρ from 1.4 to 21.4 are used.

4 Conclusions

Two different setups were proposed for the elimination of the numerical artefacts from the solution of the DMR test case. The first setup involved a modified computational domain with top and bottom boundaries normal to the shock which allowed the use of simple

Neumann boundary conditions. The second setup, on the other hand, involved a slightly modified initial shock orientation and modified Neumann boundary conditions, which allowed the use of a simple Cartesian grid. Both setups used a two-step initialization procedure to remove the spurious numerical noise generated as the initially sharp shock smears over the grid.

It has been demonstrated that both of the proposed setups are capable of eliminating the numerical artefacts to a large extent. Furthermore, it was found that the second setup is superior in performance to the first since it was able to remove the artefacts almost completely regardless of the numerical flux schemes used. It also requires a simpler computational domain and grid compared to the first one. Nevertheless, one advantage of the first setup is that the incident shock orientation with respect to the ramp surface is the same as in the conventional setup and the physical problem itself remains unchanged. Therefore, the results could be directly compared with those reported in other studies which use the conventional setup of the problem.

It is emphasized here that additional modifications need to be made to the solver in order to implement the proposed near-boundary treatment in the second setup. If the solver is optimized to run on fully structured grids, the variables are often stored as two-dimensional arrays. In such situations, the modifications expressed in equations (3) and (4) would be fairly straightforward to implement because the cell variables can be readily accessed using a two-dimensional index (i, j). On the other hand, if the solver is designed to handle generalized meshes such as in OpenFOAM, the variables are stored as one-dimensional arrays. Therefore, careful array indexing is necessary to implement the proposed near-boundary treatment in such solvers.

Vevek, U.S., Zang, B. & New, T.H. J Sci Comput (2018). https://doi.org/10.1007/s10915-018-0803-x

Acknowledgements

The authors gratefully acknowledge the support for the present work by Singapore Ministry of Education AcRF Tier-2 grant (MOE2014-T2-1-002), National Supercomputing Center Singapore (NSCC), and for the first author through Graduate Research Officer scheme from the School of Mechanical and Aerospace Engineering, Nanyang Technological University, Singapore.

References

[1] Woodward, P. and Colella, P.: The numerical simulation of two-dimensional fluid flow with strong shocks. *J. Comput. Phys.*, 54(1):115-173, (1984)

[2] Ben-Dor, G., *Shock wave reflection phenomena*. Vol. 2. 2007: Springer.

[3] Cockburn, B. and Shu, C.-W.: Runge–Kutta Discontinuous Galerkin Methods for Convection-Dominated Problems. *J. Sci. Comput.*, 16(3):173-261, (2001)

[4] Liu, H. and Qiu, J.: Finite Difference Hermite WENO Schemes for Hyperbolic Conservation Laws. *J. Sci. Comput.*, 63(2):548-572, (2015)

[5] Qiu, J. and Shu, C.W.: Runge-Kutta Discontinuous Galerkin Method Using WENO Limiters. *SIAM Journal on Scientific Computing*, 26(3):907-929, (2005)

[6] Shi, J., Zhang, Y.T., and Shu, C.W.: Resolution of high order WENO schemes for complicated flow structures. *J. Comput. Phys.*, 186(2):690-696, (2003)

[7] Shu, C.W.: High-order Finite Difference and Finite Volume WENO Schemes and Discontinuous Galerkin Methods for CFD. *International Journal of Computational Fluid Dynamics*, 17(2):107-118, (2003)

[8] Kemm, F.: On the proper setup of the double Mach reflection as a test case for the resolution of gas dynamics codes. *Computers & Fluids*, 132(Supplement C):72-75, (2016)

[9] Rider, W.J., Greenough, J.A., and Kamm, J.R.: Accurate monotonicity- and extrema-preserving methods through adaptive nonlinear hybridizations. *J. Comput. Phys.*, 225(2):1827-1848, (2007)

[10] Arora, M. and Roe, P.L.: On Postshock Oscillations Due to Shock Capturing Schemes in Unsteady Flows. *J. Comput. Phys.*, 130(1):25-40, (1997)

[11] Jiang, G.S. and Shu, C.W.: Efficient Implementation of Weighted ENO Schemes. *J. Comput. Phys.*, 126(1):202-228, (1996)

[12] Kim, D. and Kwon, J.H.: A high-order accurate hybrid scheme using a central flux scheme and a WENO scheme for compressible flowfield analysis. *J. Comput. Phys.*, 210(2):554-583, (2005)

[13] Črnjarić-Žic, N., Vuković, S., and Sopta, L.: On different flux splittings and flux functions in WENO schemes for balance laws. *Computers & Fluids*, 35(10):1074-1092, (2006)

[14] Gottlieb, S. and Shu, C.W.: Total variation diminishing Runge-Kutta schemes. *Mathematics of computation of the American Mathematical Society*, 67(221):73-85, (1998)

[15] Rusanov, V.V.: The calculation of the interaction of non-stationary shock waves and obstacles. *USSR Computational Mathematics and Mathematical Physics*, 1(2):304-320, (1962)

[16] Harten, A.: High resolution schemes for hyperbolic conservation laws. *J. Comput. Phys.*, 49(3):357-393, (1983)